Engineered Science
DOI: https://dx.doi.org/10.30919/es1150

Centrifugal Pump Optimization via Integration of Machine Learning and Computational Fluid Dynamics

Shahid Rabbani,[1, 2] Kürşad Melih Güleren[3] and Imran Afgan[1, 4,*]

Abstract

This paper presents a novel approach towards centrifugal pump design optimization, employing an integration of deep learning and Computational Fluid Dynamics (CFD). Centrifugal pumps' complex operation environments require innovative strategies for optimal performance. By harnessing machine learning, this study innovatively shifts the traditional design focus towards maximizing pressure rise and eliminating reverse flows in the impeller. The approach uses a deep learning model to predict pump performance parameters which are evaluated via comparative analysis with predefined outputs. Moreover, correlations between pressure head and relative velocity angle are investigated. Key manipulated design parameters include relative diffuser vane angle, number of diffuser vanes, number of impeller blades and the impeller wrap angle. The results demonstrate the efficacy of machine learning in delivering accurate predictions and valuable insights into pump performance, thereby paving the way for more efficient and reliable centrifugal pump designs.

Keywords: Centrifugal pump; Deep learning; Computational fluid dynamics; Optimization.
Received: 02 October 2023; Revised: 06 December 2023; Accepted: 27 January 2024.
Article type: Research article.

1. Introduction

Centrifugal pumps serve as the lifeblood in a variety of fields, including oil and gas operations,[1-6] water supply,[7,8] chemical processing,[9] wastewater management,[10] sewage/slurry disposal,[11-13] heat generation,[14-17] irrigation,[18] mining[19] and heart transplantation/cardiac operations.[20,21] They work by converting mechanical energy into kinetic energy, thereby facilitating an efficient fluid transfer process.[22] Their performance, dictating efficiency, reliability, and energy consumption, however, often finds itself at odds with complex operating environments.[23] These challenging circumstances comprise nonlinear hydraulic phenomena, fluctuating operational conditions, and external disturbances, all of which need the development of innovative strategies for optimal pump operation.

In this regard, serious efforts have been made in the optimization of centrifugal pumps for the last 15 years. Heuristic methods are frequently used in the optimization of the centrifugal pump. The remarkable works of this class; genetic optimization and experimental verification of complex parallel pump station,[24] numerical shape optimization of pump impeller using artificial bee colony algorithm,[25] multi-objective particle swarm optimization,[26] and pareto-based multi-objective optimization studies using neural networks and genetic algorithms[27] can be given as examples. It would be a mistake to design centrifugal pumps by considering one single objective. For this reason, optimization should be made by considering more than one objective. This is often referred as multi-objective optimization. For example; blockage, hydraulic efficiency, and cavitation number have been selected as the objective functions to design the impeller to reduce flow recirculation and cavitation.[28] Another shape optimization of the impeller was conducted for better pump performance.[29] Kriging metamodels, considered as one of the recently popular numerical methods, are preferred in multi-objective

[1] *Department of Mechanical & Nuclear Engineering, College of Engineering, Khalif University, Abu Dhabi, P.O.Box 127788, UAE.*
[2] *Center for Interacting Urban Networks (CITIES), New York University, Abu Dhabi, 200120, UAE.*
[3] *Eskisehir Osmangazi University, Faculty of Engineering and Architecture, Department of Aeronautical Engineering, 26040, Turkey.*
[4] *Department of Fluids and Environment, School of Engineering, University of Manchester, Manchester, M13 9PL, UK.*
**Email:* imran.afgan@ku.ac.ae, imran.afgan@manchester.ac.uk (I. Afgan)

optimizations of centrifugal pump.[30] In many multi-objective optimization studies, Computational Fluid Dynamics (CFD) plays an important role in data generation. Experimental methods, on the other hand, are used usually for validation purposes. Different optimization methods are applied to reach an optimum pump geometry. The orthogonal method, which is an important branch of statistics and widely used in industrial production and experiments, has become a preferred tool in the optimization of pump geometries by combining it with CFD. Surrogate models[31,32] and multilayer neural network[33,34] are the other methods are preferred in this field. Many examples related to optimization of centrifugal pump for industrial purposes can be given, but it should not be avoided that this field is not limited for these purposes, only. One of the interesting applications of optimization was conducted for a miniature pediatric pump to eliminate the adverse leakage flow, which is vital for heart.[32,35]

As an alternative to the variety of optimization methods and objective functions of the centrifugal pump, machine learning has emerged as a game-changing tool, offering a novel pathway to enhancing the performance of centrifugal pumps.[36-38] Machine learning algorithms utilize historical data and real-time measurements, leveraging these inputs to develop models that optimize critical operating conditions such as pump speed, impeller geometry, and flow control strategies. They bring adaptability to pump control systems, providing adaptive control strategies that continually optimize pump operations based on an analysis of evolving environments.[39-41] This dynamic approach paves the way for increased efficiency, extended equipment lifespan, and significant energy consumption reduction, collectively enhancing industrial outcomes.[42]

Additionally, machine learning, by its very nature, breaks away from the inherent limitations of traditional pump design and control methodologies, contributing to centrifugal pump performance enhancement and fault detection.[2,43-46] It negates the need for oversimplified models and assumptions, processing vast amounts of data, recognizing key features, and extracting insights that may have otherwise gone unnoticed. Machine learning algorithms learn from historical data to decipher patterns and correlations between input parameters and pump performance, resulting in more accurate predictions and a deeper understanding of the underlying physical phenomena.

A significant contribution in this regard is the implementation of reinforcement learning algorithms, which enable pumps to iteratively learn optimal control policies. This feedback-based learning allows pumps to autonomously modify their behaviour to meet operational objectives, thereby enhancing efficiency and responsiveness.[47]

The intricate flow within a centrifugal pump, characterized by high viscosity, turbulent effects, and substantial Coriolis forces, adds to the complexity of its design and optimization process. Recent advances in machine learning, when coupled with CFD techniques, have proven beneficial for addressing these design challenges in turbomachinery. These techniques are particularly beneficial when tackling the complexities of impeller-diffuser interactions within a single solution domain to generate improved designs for centrifugal pumps.

Our study hinges on this scientific progress and focuses on leveraging the prowess of advanced machine learning and CFD techniques for the optimization of centrifugal pump performance. We extend previous studies that primarily target maximizing efficiency and minimizing Net Positive Suction Head required (NPSHr). Instead, our work aims at maximizing the pressure rise ΔP and eliminating reverse flows in the impeller to offer a fast solution from the CFD perspective.

We undertake a comprehensive approach, modifying pump geometry based on parameters like the relative diffuser vane angle α_{dif}, number of diffuser vanes Z_d, number of impeller blades Z_i, and the impeller wrap angle α_{wrap}. In this study, we mainly focus on the impeller and diffuser blade orientations. The impeller diameter is kept constant but with changes to the different wrap angles which leads to variable outlet angles (the center of the diffuser vanes is kept fixed, however, by rotating the diffuser angle vanes around the fixed diffuser center provides variable inlet and outlet diffuser angle. Therefore, the chosen design parameters in essence provide different inlet and outlet angles). Our study stands apart in its unique approach to deep learning, which integrates the CFD solution of a centrifugal pump based on impeller-diffuser matching using these parameters, a methodology not explored before, to the best of our knowledge

This paper presents an empirical model derived from numerical simulations of 693 combinations of these parameters to optimize relative velocity angle and pressure head. The data points from these simulations serve as inputs for a deep learning model to predict pressure head and relative velocity. We also conduct exploratory data analysis of this data and present the findings. Through this study, we aim to establish significant correlations between pressure head and relative velocity angle that can drive future engineering efforts in centrifugal pump design.

Firstly, we present the numerical simulations we conducted to acquire the requisite data. These simulations, involving 693 different combinations of the key design parameters relative diffuser vane angle α_{dif}, number of diffuser vanes Z_d, number of impeller blades Z_i, and the impeller wrap angle α_{wrap} -serve

as the foundation of our study. The outputs of these simulations provide us with data on pressure head and relative velocity angle, which are critical to the optimization of centrifugal pump performance.

Following the data acquisition, we delve into an extensive exploratory data analysis (EDA) of the simulation results. This step is crucial to our understanding of the data's structure and identifying patterns and relationships between the variables. By visualizing and summarizing the data, we seek to generate insights that can further guide our predictive modelling efforts. After the EDA, we present our deep learning model that utilizes the data obtained from the numerical simulations. This advanced machine learning model is developed to predict pressure head and relative velocity angle, key performance indicators of centrifugal pump performance. By learning from the extensive data generated from the numerical simulations, the model aims to provide accurate predictions and a deeper understanding of the relationship between the design parameters and pump performance.

Subsequently, we introduce the correlation analysis conducted to predict the pressure head and relative velocity angle. Here, we aim to uncover any significant correlations for pressure head and relative velocity angle, which can be instrumental in future engineering and optimization efforts.

Finally, the paper culminates in a conclusion where we recapitulate our findings, discuss their implications, and suggest directions for future research in the area. This section is designed to summarize the research and provide a clear understanding of its significance and potential future applications.

2. CFD Case Setup

In this section, the methodology adopted for the creation of the pump geometry, flow solver, and grid structure are explained.

2.1 Geometry and grid

The centrifugal pump investigated in the present study has been experimentally studied in the past by Ref. [48]; the turbulent flow behaviour was investigated using 2D particle image velocimetry (PIV). A schematic description of the pump geometry, location of measurements and sample area are presented in Fig. 1. To ensure smooth flow into the pump, a settling chamber, honeycombs, screens, and turning vanes were employed. To minimize vibrations and isolate the pump from the rest of the facility, 50 meters of coiled flexible hoses were utilized. The test model consisted of a vertical centrifugal pump equipped with a vaned diffuser, operating at 890 rpm. The pump's design specific speed was 0.49, with an estimated design flow coefficient of 0.118 and a head coefficient of 5.2. As depicted in Fig. 1, the impeller features five backward-swept blades with a logarithmic profile, each with an exit angle of 19 degrees relative to the tangent. At the inlet, the impeller blade inlet angle at the hub relative to the circumferential tangent was 14.1 degrees, while the blade inlet angle at the shroud surface was approximately 24.2 degrees. The impeller's inlet and discharge blade tip diameters were 8.51 and 20.32 centimeters, respectively. The optical setup of the PIV system is given in Fig. 2. To provide unobstructed visibility of the flow within the transparent sections of the impeller, the gap between the rotor and stator, the diffuser vanes, and the volute, the facility was meticulously designed. A combination of cylindrical and spherical lenses was utilized which expanded the laser beam into a 1-millimeter-thick light sheet. This sheet illuminates any desired section of the volute through the transparent perimeter. Illumination from below was also possible to examine normal locations. The image was captured by a camera positioned below the pump. Two types of lasers were employed: a continuously pulsed copper vapor laser with primary wavelengths of 511 and 578 nm, and a frequency-doubled Nd-YAG laser operating at 532 nm. The majority of experiments were conducted using the Nd-YAG laser. For detailed information about the experimental setup and the outputs please see [48].

The geometry and the corresponding grid topology for the present study were generated using Gambit 2.4.6[49] software based on the dimensions given in Table 1 and illustrated in Fig. 3.

Geometries were generated via a Gambit journal file. The algorithm for the journal file is tabulated in Table 2.

For each CFD simulation, the journal file was created from scratch based on the values of the parameters used for deep learning. Values change from -5° to 10° for the relative diffuser angle, from 8 to 10 for the number of diffuser vanes, from 4 to 6 for the number of impeller blades, and from -10° to 15° for the impeller wrap angle. The geometrical orientation of the wrap and relative diffuser angles are schematically shown in Fig. 4. The ranges of the parameters are determined in such a way that automatic generation of the diffuser vanes and the impeller blades do not intersect. In order words, the leading and trailing edges of the diffuser vanes do not extend into the impeller volume. As for the grid topology employed in this study, firstly a pave-type inviscid grid was created. Then the grid was exported to Fluent solver. The solver uses a hanging-node adaptation for every 200 iterations near the walls (impeller blades, diffuser vanes, and the volute) to predict the boundary layer effect. Therefore, the flow solver has a part in the role of grid formation in this study.

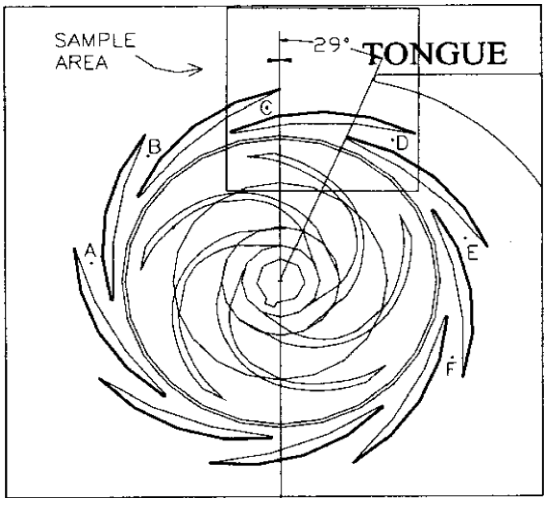

Fig. 1 The centrifugal pump geometry. Reproduced with the permission from [48], American Society of Mechanical Engineers.

2.2 Flow solver

The governing transport equations were solved via a multi-purpose finite-volume code, Fluent 6.3.26[50] solver, based on the projection method.[51] The flow was assumed to be steady, viscous, and incompressible. The frozen rotor approach was employed for the flow in the impeller. Second-order upwind schemes were used for the equations of momentum, turbulent kinetic energy, and turbulence dissipation. An under-relaxation factor of 0.3 for pressure was used to avoid numerical instabilities. PISO[52] algorithm and PRESTO[53] scheme were adopted for the pressure–velocity coupling and the pressure interpolation, respectively. For the simulations, the $k-\omega$ SST turbulence model[54] was adopted. This model combines the strength of the near wall behavior of $k-\omega$ model and numerical robustness of the $k-\epsilon$ model in the far field. The model has been successfully tested and benchmarked for several past studies, with rotating turbomachinery.[55-57] The linearized equations were solved by the Gauss-Seidel method with an algebraic multigrid method to accelerate convergence. Similar to the grid generation, the flow solver was run using a journal file. Constant mass flow rate and pressure were imposed at the inlet and exit boundary conditions, respectively. After the convergence was achieved, pressure head and the relative angle in the impeller were calculated. The algorithm adopted for the Fluent journal file is given in Table 3.

Table 1. Dimensions of the original pump. Reproduced with the permission from [48], American Society of Mechanical Engineers.

Impeller inlet diameter	8.51 cm
Impeller discharge diameter	20.32 cm
Diffuser inside diameter	24.45 cm
Diffuser chord length	30.5 cm
Diffuser suction side radius	13.44 cm
Diffuser pressure side radius	14.15 cm
Diffuser discharge diameter	24.79 cm
Number of impeller blades	5
Number of diffuser vanes	9
Impeller wrap angle	170°

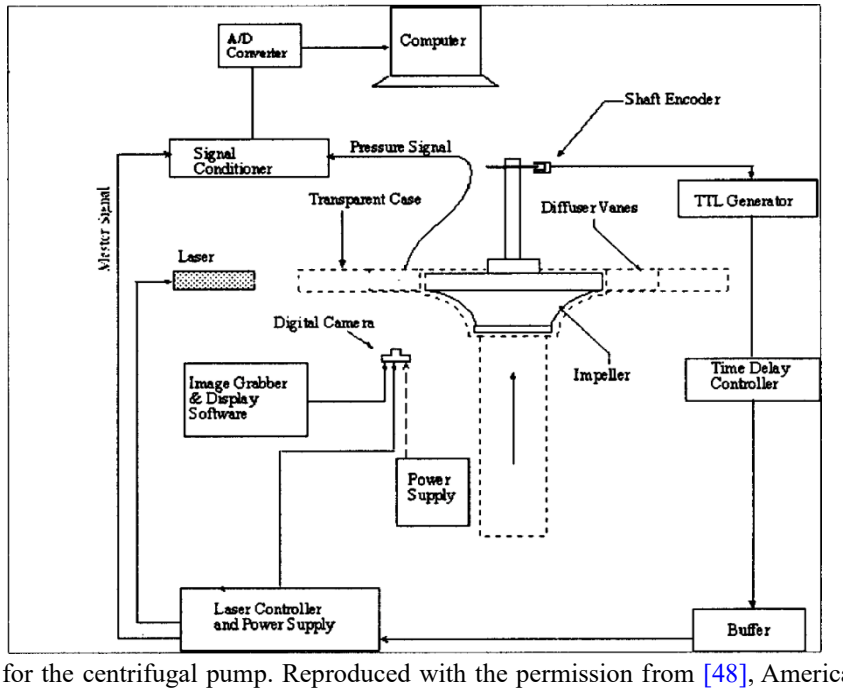

Fig. 2 Experimental setup for the centrifugal pump. Reproduced with the permission from [48], American Society of Mechanical Engineers.

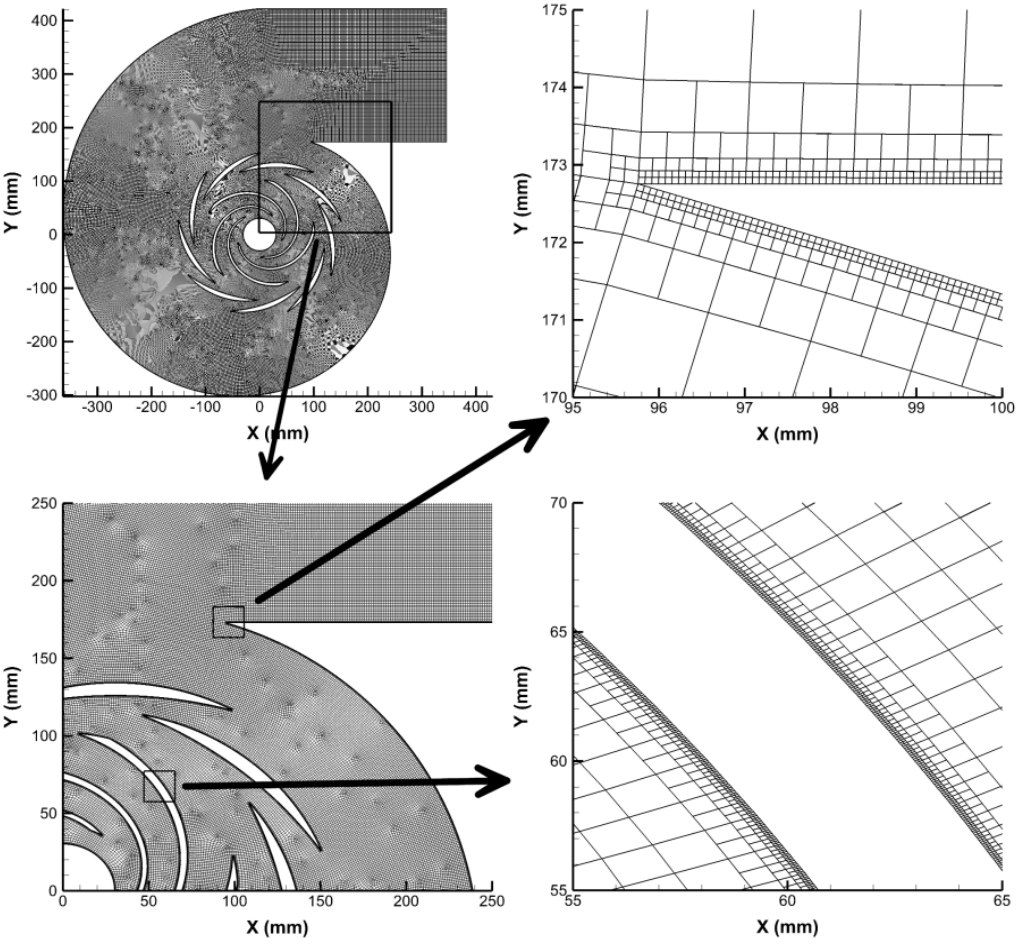

Fig. 3 Adopted grid structure for flow analyses.

Table 2. Algorithm for the geometry and grid generation.

Step Number	Action
1	Reference coordinate system is activated for the impeller.
2	Ten vertices are generated on the suction side of the original impeller blade by dividing the edge with equidistance lengths.
3	These vertices are copied based on the wrap angle by rotating around the impeller centre (0,0).
4	A nurb-type edge is created by the interpolation of these ten vertices.
5	Pressure side is created via the rotation of the suction side by rotating with the impeller centre (0,0).
6	Leading and trailing edges are created.
7	Impeller blade is created from leading, trailing, pressure side, and suction side edges.
8	Impeller blade is copied based on the desired number of blades by rotating around impeller centre (0,0).
9	Alternative coordinate system is activated for the vaned diffuser.
10	A diffuser vane is created based on the diffuser angle relative to the original diffuser vane.
11	Diffuser vane is copied based on the desired number of vanes.
12	Impeller region is meshed.
13	Diffuser and volute region is meshed.
14	Interior region is defined for the impeller.
15	Interior region is defined for the diffuser and volute.
16	Exterior regions (inlet, outlet, volute walls, impeller and diffuser vanes) are defined.
17	Mesh file is exported.

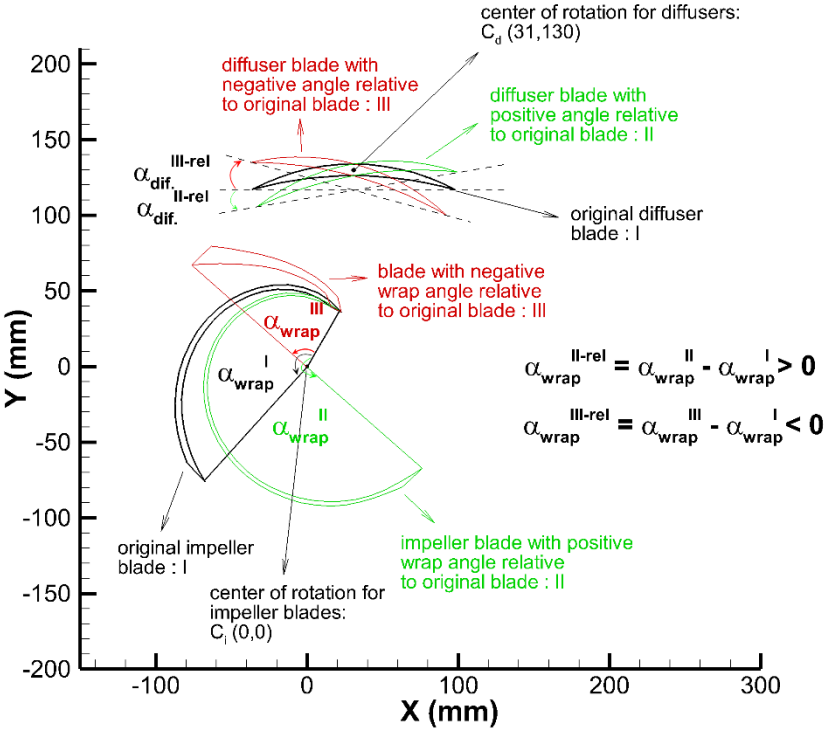

Fig. 4 Definition of impeller wrap angle (α_{wrap}) and relative diffuser vane angle (α_{dif}). C_i is the centre of the impeller and C_d is the centre of mean camber of the diffuser vane.

Table 3. Algorithm for the flow solution.

Step Number	Action
1	Mesh file is read into flow solver.
2	Reference density is set as the water density.
3	Reference fluid region is set as the impeller region.
4	Grid is scaled.
5	Material properties are set for the interior regions.
6	Impeller region is set as rotational (93.2 rad/s).
7	Turbulence model is selected.
8	Outlet boundary is set as Dirichlet boundary (constant pressure is applied).
9	Inlet boundary is set as Dirichlet boundary (constant mass flow rate is applied).
10	Convergence criteria are selected as 10^{-4}.
11	Flow field is initiated.
12	Solution is started with 200 iterations. Three stages of y^+ adaptation is employed. Cartesian grid is applied next to the walls for every 100 iterations to reach an average y^+ value of 30.
13	Pressures at the inlet and outlet regions is written in a file.

2.3 Mesh sensitivity and benchmark comparisons

A total of 693 CFD cases were run for the analysis of deep learning. Before the runs, a mesh sensitivity study was performed. For this, four types of grids were used. A schematic comparison of tested grids is shown in Fig. 5. The first type grid, which was referred as coarse grid, has an inviscid mesh without any boundary layer adaptation. The second type grid has a mild adaptation near the walls and in the entire domain. The grid size is around 1.5 times the size of the coarse grid. The third type grid has a better boundary layer adaptation but a mild refinement for the rest of the domain. The cell size is around 2 times the first type grid. The fourth type is the finest mesh where the grid is refined maximum near the walls as well as for the rest. The cell size is around 4 times the coarse grid.

It is of utmost important to know the sensitivity of the solver since reliable data is required for a deep learning study. It is not documented here, but the solver was seen to show almost no difference in pressure predictions in the case of

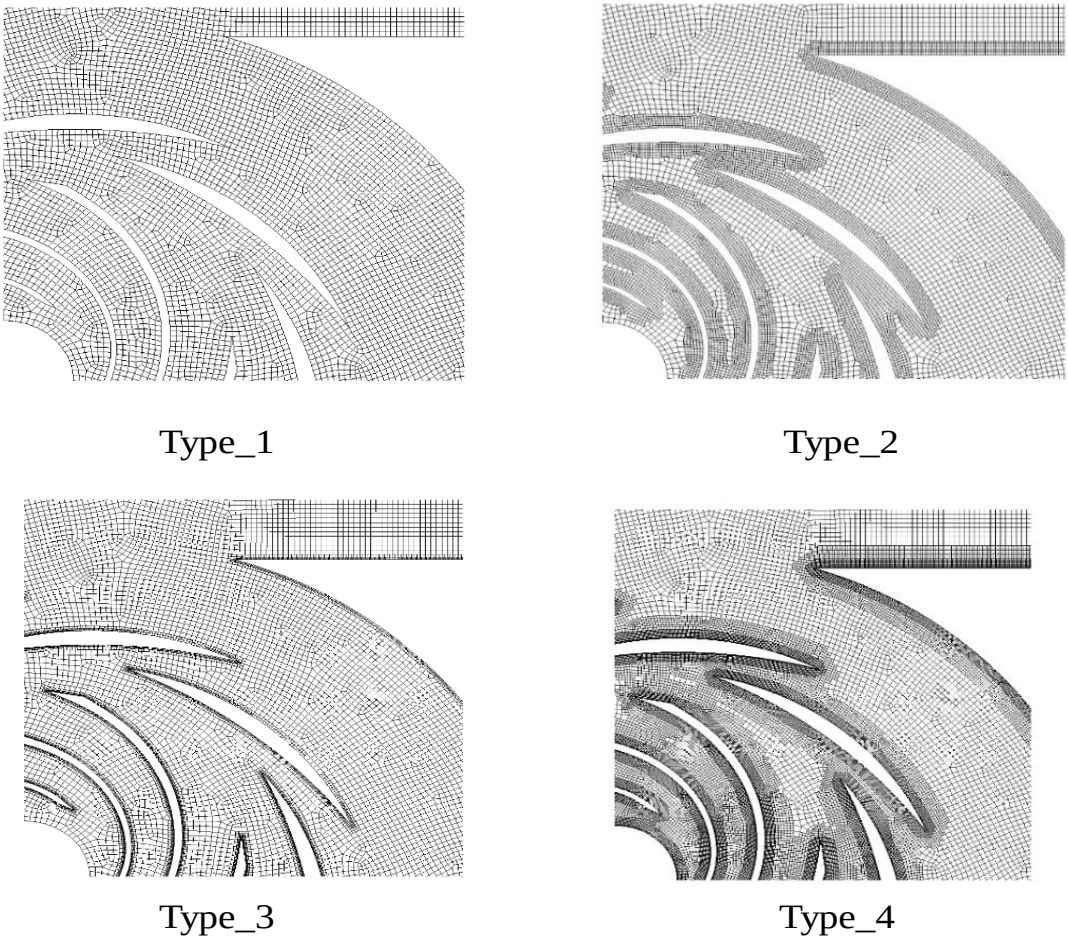

Fig. 5 Schematic comparison of tested grids (Type_1: Coarse Grid, Type_2: Medium Grid, Type_3: Fine Grid, Type_4: Very Fine Grid).

different boundary conditions, extended inlet and outlet boundaries and different two-equation RANS models. However, the grid resolution was thought as a major factor for the results. To understand the effect of grid resolution, as mentioned, four types of grids were tested for the original pump configuration.[48] Details of the various parameters for these meshes and relative errors with the finest mesh are shown in Table 4. It can be seen that the relative errors of Type_2 and Type_3 meshes compared to Type_4 mesh were within 1% for minimum pressure, maximum pressure and minimum relative velocity configurations. However, for the maximum velocity configuration Type_3, parameter predictions were much closer to the Type 4 mesh and hence this Type_3 mesh was then used for all future simulations. Apart from the quantitative comparisons of different meshes, we also looked at the flow physics as to which mesh was performing better. For this purpose, the pressure and the hydraulic power results are compared with the available experimental data as seen in Fig. 6. As shown, tested grids over-predict the pressure values at low mass flow rates, due to the significant turbulent behaviour which results when the pump is driven to off-design conditions at low flow rates (stagnation). Discrepancies decrease at high mass flow rates. Over results of Type_1 and Type_2 suggest that the boundary layer refinement might be necessary to obtain better predictions. As for the power results, there is a good agreement between the predictions and experimental data for low mass flow rates till 2.6 kg/s. After this, Type_1 and Type_2 results seem to differ from the experimental data, significantly. Type_3 improves both pressure and power predictions similar to Type_4. Therefore, it can be concluded that the grid convergence is achieved and as a result, Type_3 is considered as a reasonable choice for the CFD runs. It should be noted that, since the 3D pump geometry is very complex and CFD runs are very time-consuming, the optimization has been performed with 2D CFD cases. To validate the numerical setup and flow model, pressure and power predictions for a 3D CFD run are included in Fig. 6. As shown in Fig. 6, the predictions for the 3D configuration agree well with both pressure and power data of the experiment, within 2% whereas the 2D numerical data was within 8% of the experimental data as shown by the error bars in this plot. After the CFD runs, the effect of tested grids on some distinctive cases was examined to be confident about the grid independence. Out of 693 runs, four cases were chosen: minimum and maximum outputs for pressure head and relative impeller angle. As seen in Fig. 6,

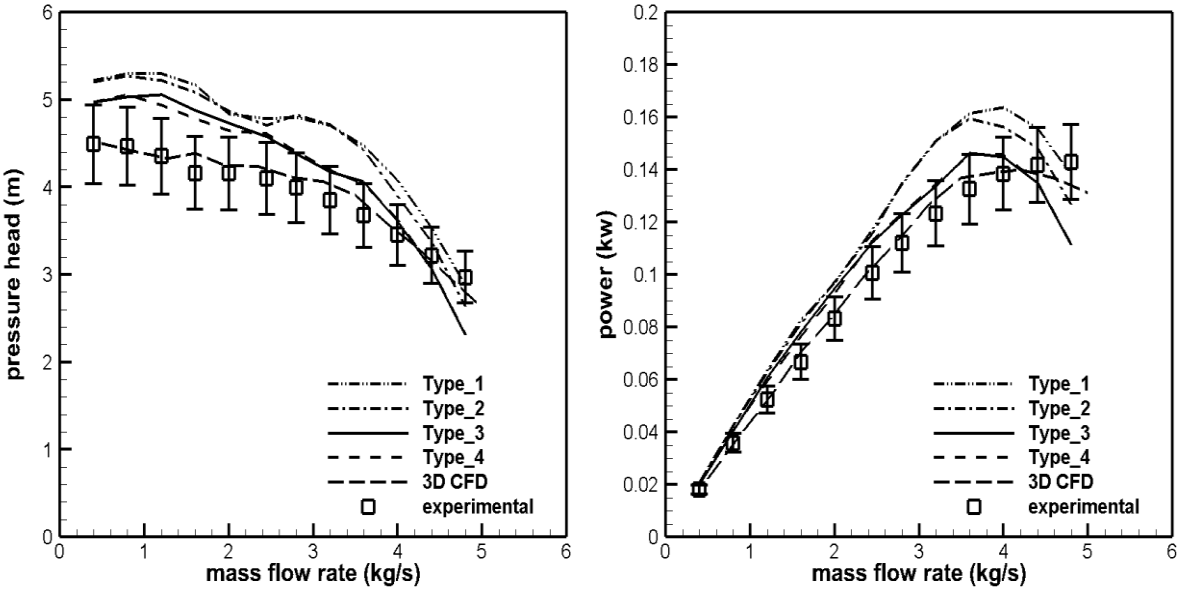

Fig. 6 Mass Flow Rate and Hydraulic Power Comparison for the grids and the experimental data.[48]

Type_3 and Type_4 grids predict very close values for all distinctive cases, therefore the use of Type_3 grid for CFD runs has been an appropriate choice. It is important to mention here that the useful set of data configurations out of the total 693 was only 525; cases which returned a positive pressure head. The reason behind this is that when the original range of design parameters were chosen (relative diffuser vane angle α_{dif}, number of diffuser vanes Z_d, number of impeller blades Z_i, and the impeller wrap angle α_{wrap}), we did not anticipate a-priori if the output of the pump would be negative or positive; we only had to option to define the range of the varying parameter based on the geometric constraints, as already aforementioned. Thus, the total number of useful cases was reduced to 525, which are used for the machine learning part for the later analysis.

3. Exploratory Data Analysis (EDA)

The dataset generated via the CFD simulations consists of four (4) predictor variables (*i.e.*, impeller wrap angle, relative diffuser angle, number of diffuser vanes, and number of impeller blades). These were used to predict pressure head and relative velocity angles. Fig. 7 shows a comprehensive representation of the 693 data points, illustrating the relationship between key parameters in the centrifugal pump system. Here the x-axis represents the data points, while the y-axis depicts the impeller wrap angle, no. of diffuser vanes,

Table 4. The effect of grids on distinctive cases with relative errors.

		Type_1		Type_2		Type_3		Type_4
		Coarse Mesh	Error %	Medium Mesh	Error %	Fine Mesh	Error %	Very Fine Mesh
Minimum Pressure Case	Cells (*10^3)	132.00	-	224.00	-	273.00	-	517.00
	Pressure (m)	-9.6	8.82	-10.54	0.02	-10.64	-0.98	-10.55
	Rel. Vel. Angle (°)	-89.40	-0.22	-89.20	0.01	-89.30	-0.11	-89.20
Maximum Pressure Case	Cells (*10^3)	103.00	-	143.00	-	223.00	-	449.00
	Pressure (m)	5.27	-4.08	5.16	-2.04	4.96	2.04	5.06
	Rel. Vel. Angle (°)	-88.10	0.23	-87.80	0.57	-87.90	0.45	-88.30
Minimum Relative Velocity Angle Case	Cells (*10^3)	106.00	-	145.00	-	225.00	-	454.00
	Pressure (m)	5.06	-4.26	4.96	-2.13	4.75	2.13	4.85
	Rel. Vel. Angle (°)	-90.00	0.00	-90.00	0.00	-90.00	0.00	-90.00
Maximum Relative Velocity Angle Case	Cells (*10^3)	100.00	-	138.00	-	216.00	-	440.00
	Pressure (m)	5.27	-8.51	5.06	-4.26	4.96	-2.13	4.85
	Rel. Vel. Angle (°)	-86.20	-1.41	-86.40	-1.65	-85.50	-0.59	-85.00

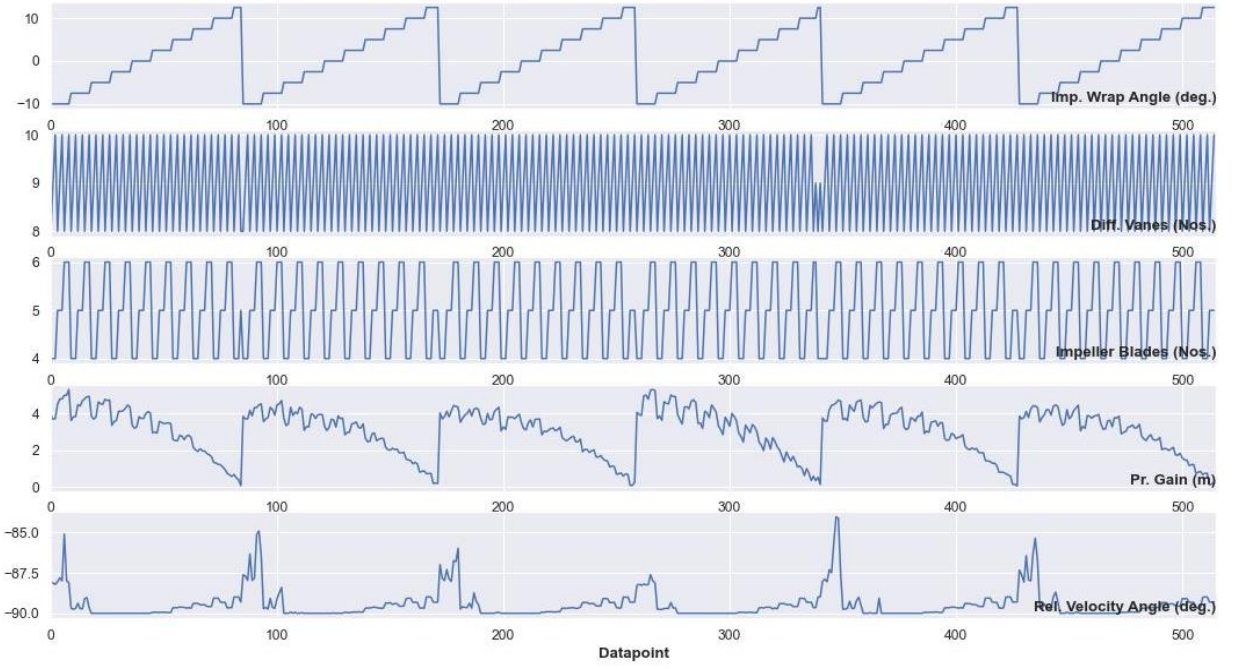

Fig. 7 Data points of the given dataset for the impeller wrap angle, no. of diffuser vanes, pressure head, and relative velocity angle.

pressure head, and relative velocity angle, respectively. This figure provides a concise visual overview of the intricate connections between these parameters, offering valuable insights into their interdependencies within the pump system. connections between these parameters, offering valuable insights into their interdependencies within the pump system.

Figure 8 gives the interplay between the impeller wrap angle, number of diffuser vanes, pressure head, and relative velocity angle in the centrifugal pump system. Correlations (see Fig. 9) and patterns emerge from the carefully arranged scatter plots, enriching our understanding of these parameters' impact on pressure head and relative velocity angle.

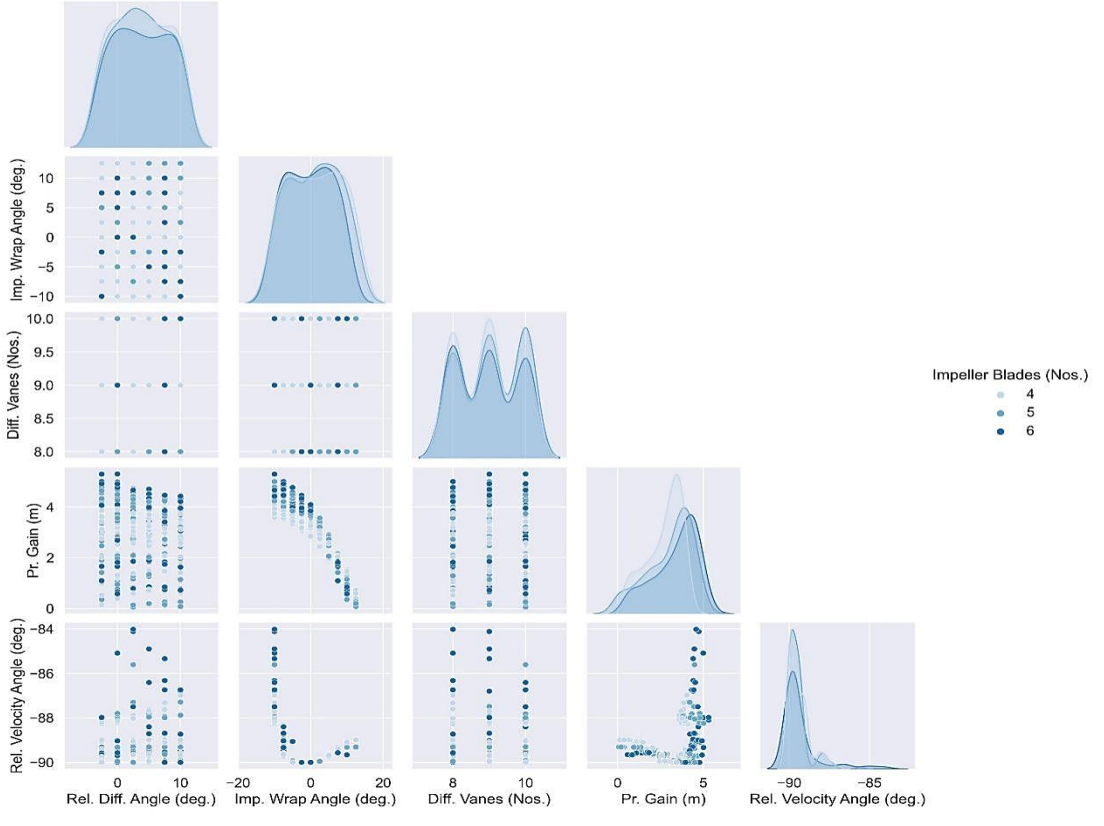

Fig. 8 Relationship displayed using scattered and kde plots between different data values.

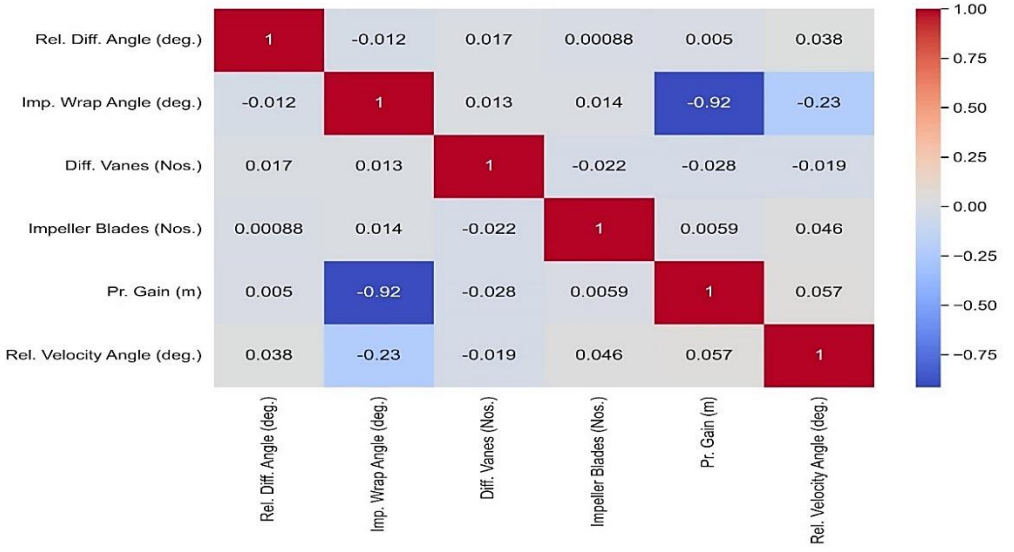

Fig. 9 Correlation matrix for predictor variables.

The correlation matrix (Fig. 9) reveals significant associations between pressure head, relative velocity angle, and the impeller parameters, specifically the impeller blades and impeller wrap angle. This indicates a strong relationship between these variables in the centrifugal pump system. The findings suggest that variations in impeller design, such as the number of blades and wrap angle, have a direct influence on both pressure head and the relative velocity angle (see Fig. 9 in conjunction with Fig. 10). Understanding these relationships is crucial for optimizing pump performance and achieving desired operational goals in various applications.

4. Modelling using deep learning

In the exploration of a pressure prediction model, we formulated the deep learning model utilizing the Keras framework. The dataset was divided using an 80/20 partitioning scheme, where 80% of the data was designated for training, and the remaining 20% was allocated for validation purposes.

Prior to the implementation of the model, the data was

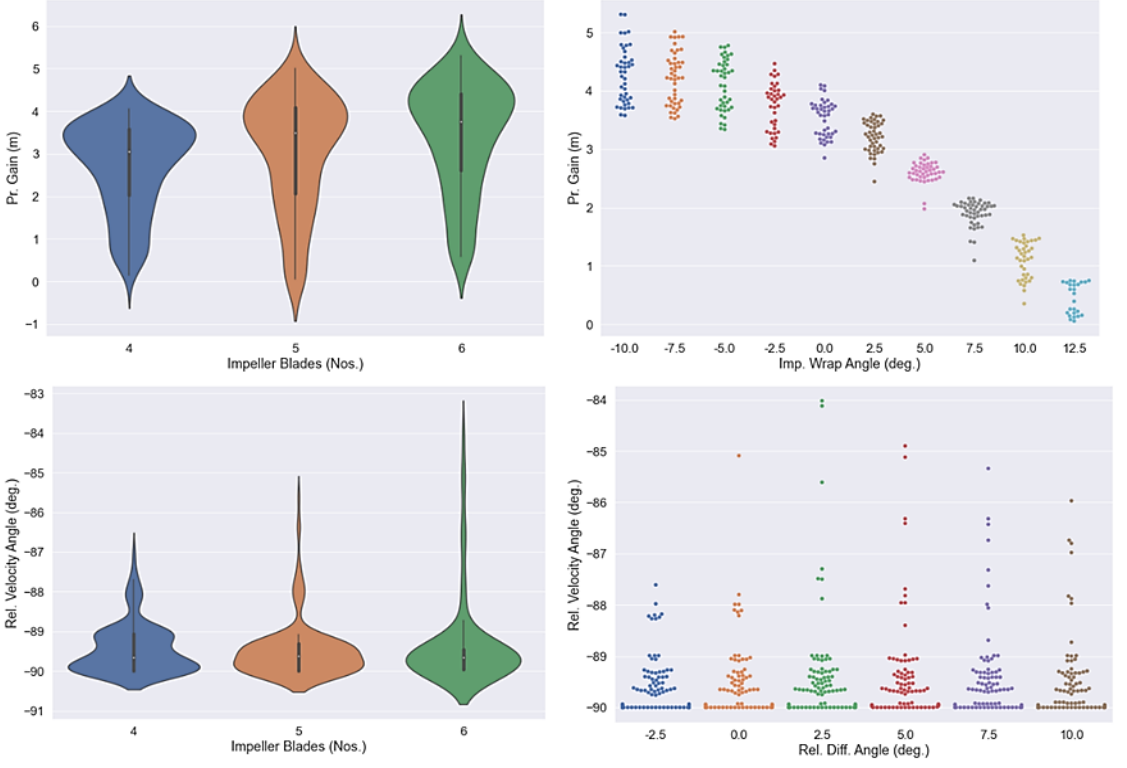

Fig. 10 Violin plot (left) and Swarm plot (right) for features which are strongly correlated with Pressure Head and Relative Velocity Angle.

initially normalized to eliminate the potential influence of differing scales or magnitudes, thereby improving the efficacy of the learning process. Subsequently, we employed a sequential model from Keras, featuring a robust architecture of nine layers, which was instrumental in capturing complex patterns and relationships within the data.

To quantify the quality of the model during the training process, we selected Mean Squared Error (MSE) as the loss function for pressure head model. The MSE function provides a suitable and effective method of determining the average squared difference between the predicted and actual values, thereby ensuring an optimal fit of the model to the data.

In terms of optimization, the Adam optimizer was selected, a popular choice owing to its efficiency and low computational requirement. Adam combines the advantages of two other extensions of stochastic gradient descent: Adaptive Gradient Algorithm (AdaGrad) and Root Mean Square Propagation (RMSProp), thereby ensuring efficient and effective model optimization. Overall, a nine-layer Sequential model using the MSE loss function and the Adam optimizer, pressure prediction model was trained up to 1000 epochs (see Fig. 11).

The data associated with the relative velocity angle exhibited a particularly narrow range (see Fig. 7). Given this characteristic, a model that incorporated the Leaky Rectified Linear Unit (LeakyReLU) activation function was determined to be sufficiently effective in achieving reliable predictions. The LeakyReLU function was chosen because it offers a solution to the 'dying ReLU' problem, allowing for a small, positive gradient when the unit is not active and thus facilitating improved learning from the data with less substantial variation.

For the purpose of error calculation, the Huber loss function was selected. Huber loss (also called Huber error) is a loss function used in regression tasks that combines the best properties of mean squared error (MSE) and mean absolute error (MAE). Like MSE, it penalizes large errors more than small errors, but like MAE, it is less sensitive to outliers. The Huber loss function is defined as:

For $|y_{pred} - y_{true}| <=$:0.5 x $(y_{pred} - y_{true})^2$

For $| y_{pred} - y_{true} | >$: x $| y_{pred} - y_{true} |$ - 0.5 * ^{2}

where y_{pred} is the predicted value, y_{true} is the true value, and delta is a hyperparameter that determines the point at which the loss switches from quadratic to linear. If the absolute difference between the predicted and true values is less than delta, the loss is quadratic, otherwise it is linear. Huber loss can be used as a drop-in replacement for MSE in many cases and can improve the robustness and stability of the model, especially in the presence of outliers.

To achieve an optimal fit, the model was trained over 1,000 epochs (see Fig. 12). This extended training period allowed the model to thoroughly learn and extract the underlying patterns within the data, thereby facilitating more accurate and reliable predictions.

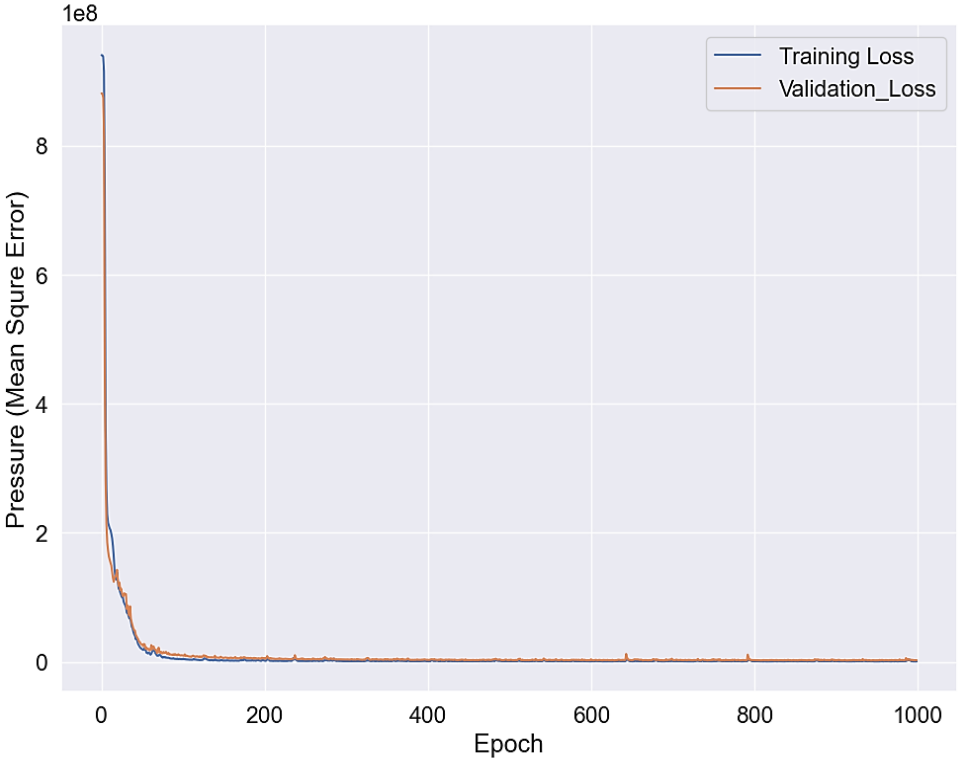

Fig. 11 Evolution of MSE with number of epochs for pressure.

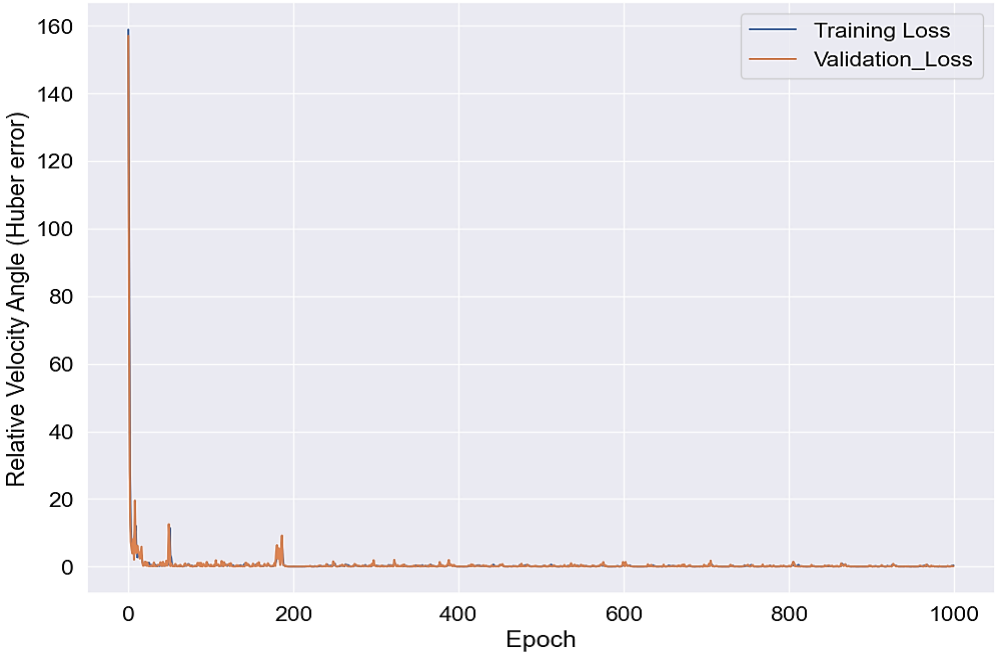

Fig. 12 Evolution of error with number of epochs for relative velocity angle.

5. Results

5.1 Pressure predictions using deep neural network

To evaluate the performance of the trained model, the predicted pressure values were compared with a validation dataset. This dataset is distinct from the training dataset and is used to assess the model's generalization ability, *i.e.*, its capability to predict accurately on unseen data. The comparison results are illustrated in Fig. 13. In this figure, the points located above and below the diagonal line respectively signify instances where the model overpredicts and underpredicts the pressure values. The ideal model would produce points that align perfectly with the diagonal line, indicating that predicted values are equal to the actual values. Further insight into the model's performance is provided in Fig. 14, where the error margin for the majority of the data points tested on the validation dataset is shown to be zero or close to zero. This indicates that the model has a high degree of accuracy, as a low error margin signifies that the model's predictions are very close to the actual values.

In addition to the graphical representation, we also computed quantitative evidence to support the model's performance. The Mean Absolute Percentage Error (MAPE)

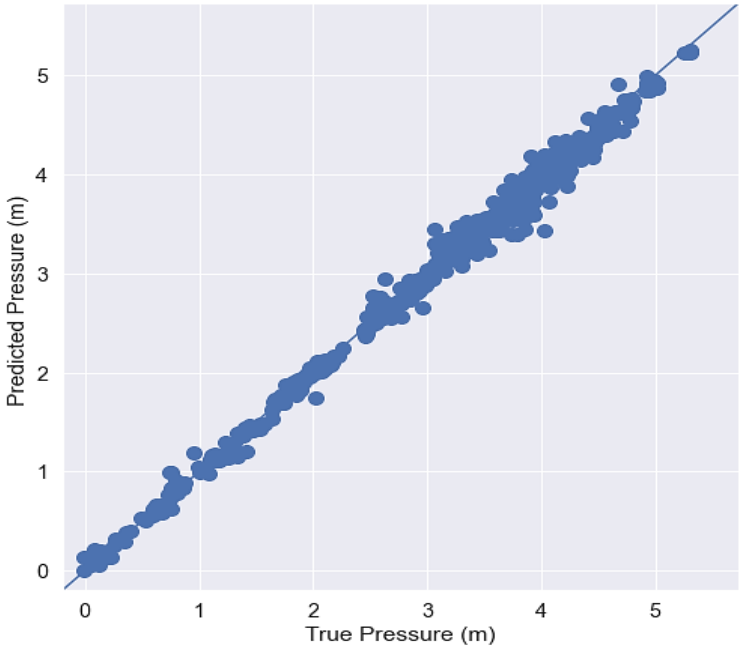

Fig. 13 Comparison of true vs predicted values for validation dataset for pressure.

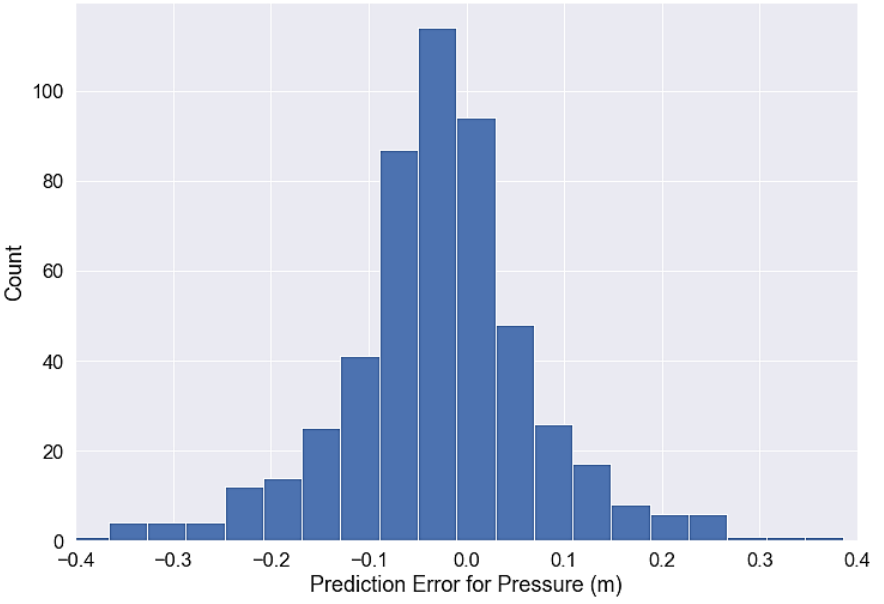

Fig. 14 Histogram for prediction error for Pressure validation data set.

was calculated for the validation dataset and found to be 6.83%. MAPE is a measure that expresses prediction errors as a percentage of the actual values, providing a scale-independent measure of prediction accuracy. A lower MAPE value signifies better model performance. Furthermore, it was observed that 87.15% of the predictions for the validation dataset had an error within ±10%. This high percentage suggests that the majority of the model's predictions are within a reasonable error margin, reinforcing the model's strong predictive performance.

5.2 Pressure Correlation

Correlation to predict pressure P (pascals) was found to be:

$$\begin{aligned} P = -25818.86 - 693.3d + 1331.25w + 12448.2v \\ + 11992.6b - 309.6d^2 + 58.43dw \\ + 1140.37dv - 125.89db - 103.41w^2 \\ - 63.15wv - 520.31wb - 1132.37v^2 \\ + 259.81vb - 1214.19b^2 \end{aligned}$$

where, d is the relative diffuser vane angle (α_{dif}) in degrees, w is the impeller wrap angle α_{wrap} in degrees, v is the number of diffuser vanes (Z_d), and b is the number of impeller blades (Z_i).

Our analysis revealed a significant correlation between pressure head and the selected predictor variables. To better understand the relationship between the true pressure and predicted pressure, we present Fig. 15, which visually compares these two variables. The graphical representation in Fig. 15 demonstrates a strong positive linear relationship, indicating that our model accurately predicts pressure head based on the selected predictor variables.

To quantitatively assess the strength and direction of the correlation, we calculated Pearson's correlation coefficient (r). Our analysis yielded an r-value of 0.94, suggesting a strong positive correlation between true pressure and predicted pressure. This high correlation coefficient implies that our model is highly effective in predicting pressure head with a minimal degree of error. The close proximity of the r-value to 1 indicates that our model accounts for a significant proportion of the variance in pressure head, further validating its accuracy and reliability in this context.

5.3 Relative velocity angle prediction

Figure 16 provides a graphical comparison between the predicted relative velocity angle and the true relative velocity angle. The majority of the points lie along the diagonal line, which suggests a satisfactory level of accuracy in our model's predictions. The diagonal alignment signifies that the predicted values are, for the most part, equal to the true values. This strong alignment is indicative of the model's high predictive accuracy.

Figure 17 further validates the efficacy of our model by evaluating prediction errors via a histogram. The majority of prediction counts are centred around 0, which indicates a minimal deviation between the predicted and true values. This distribution of prediction errors also underscores the model's high accuracy and ability to consistently produce reliable results.

Quantitatively, the mean absolute error (MAE) of the validation dataset is only 0.025%, which is exceedingly low. This minimal error rate attests to the model's excellent performance and predictive precision. Furthermore, 100% of the validation dataset had an error within ± 5%, which once again affirms the model's reliability and accuracy.

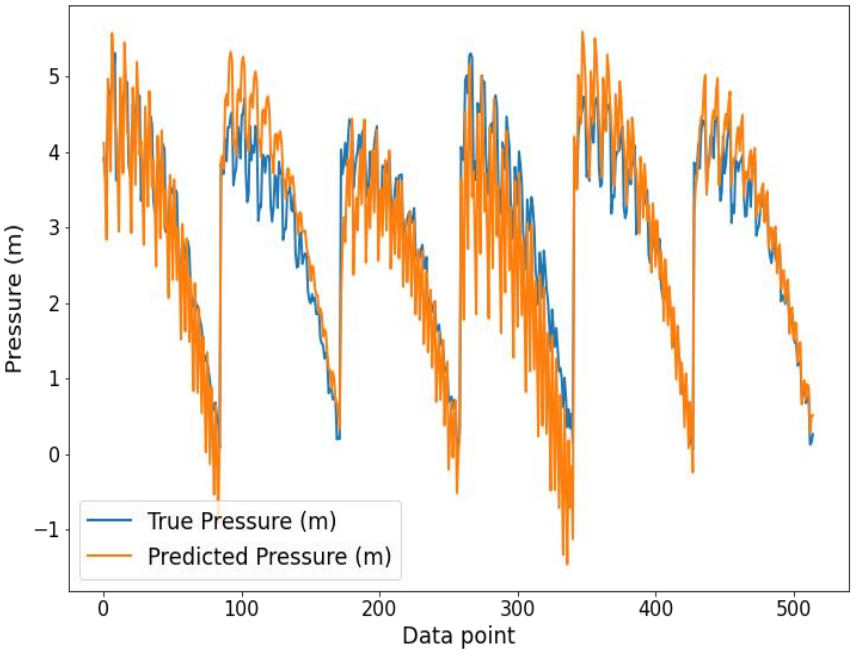

Fig. 15 Comparison of true pressure values vs the values predicted by correlation.

5.4 Relative velocity angle correlation

Correlation to find relative velocity angle *(r)* was found to be:

$$r = -89.96 + 0.28d + 0.13w - 0.09b + 0.08db - 0.02v^2 + 0.49vb - 0.44b^2$$

Our analysis reveals a strong and significant correlation between the relative velocity angle and the predicted velocity angle. The Pearson correlation coefficient, a measure of the linear correlation between these two variables, was found to be 0.90, indicating a robust positive relationship.

As depicted in Fig. 18, there is a close alignment between the relative and predicted velocity angles. This close association suggests that our predictor variables are effectively capturing the dynamics that drive the relative velocity angle.

5.5 Optimal case

To find out whether the application of machine learning in the centrifugal pump gives a successful result, three points (configurations) from Fig. 15 with pressure drops of 2 m, 3 m and 4.5 m were selected and analyses were carried out to obtain the pressure head and performance curve for these points. The geometric properties for these points are presented in the Table 5. It can be seen from Fig. 19 that the pump

Fig. 16 Comparison of true vs predicted values for validation dataset for relative velocity angle.

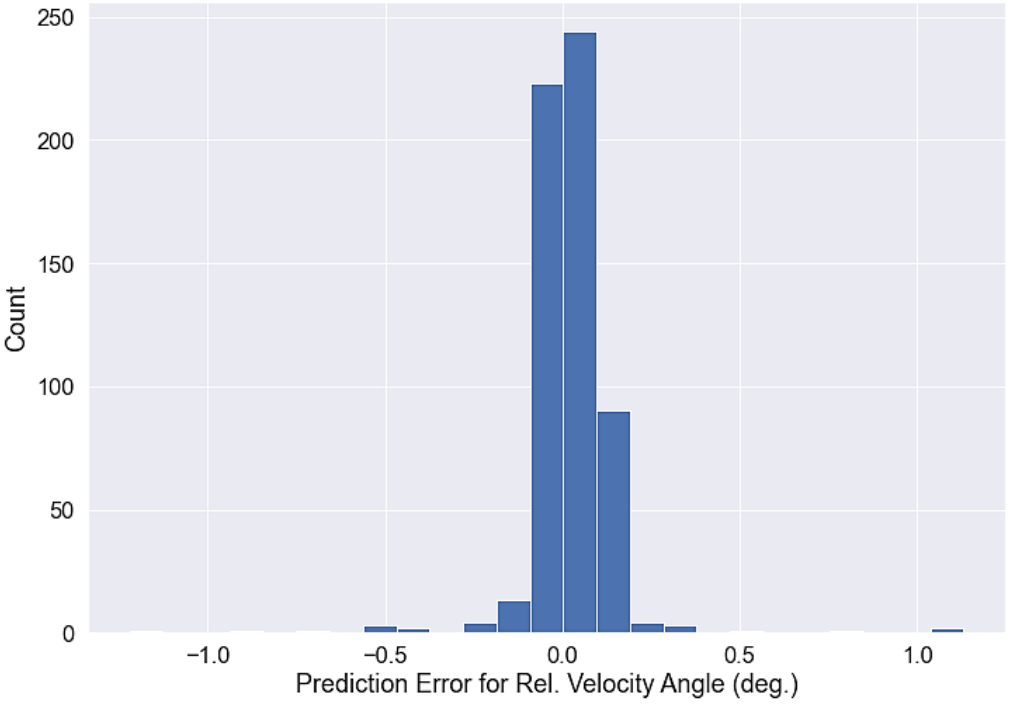

Fig. 17 Histogram for prediction error for Relative Velocity Angle validation data set.

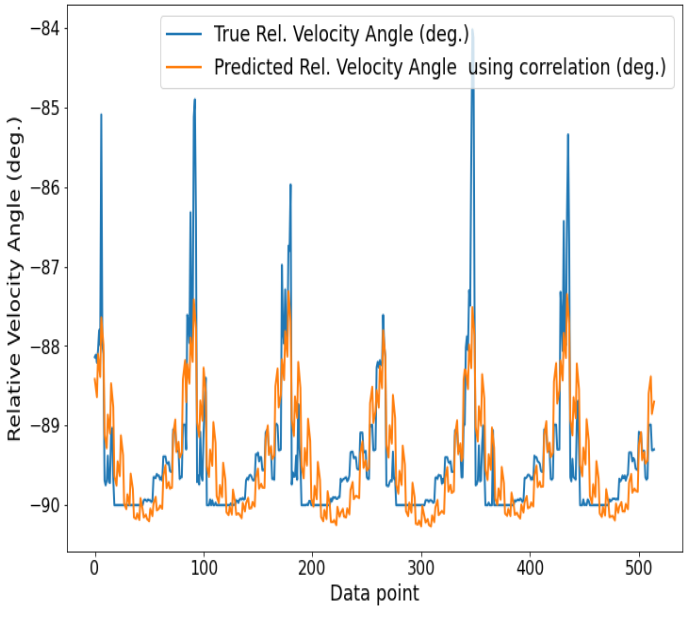

Fig. 18 Comparison of true relative velocity angle values vs the values predicted by correlation.

geometry selected as configuration 3 provided a higher-pressure head and better performance compared to the original geometry and other geometries at both low and high flow rates. While the flow rate decreases very sharply with the increase in mass flow rate in the original and other geometries, there is a slower decrease for configuration 3. This can be clearly observed from the performance curve. So much so that, while it reaches maximum power very early in the original and other geometries, the power increase continues for configuration 3. Therefore, it can be concluded that configuration 3 is one of the optimal geometries that is achieved via the machine learning analysis.

Table 5. Geometric properties of selected geometries from machine learning.

	Rel. Diff. Angle (deg.)	Imp. Wrap Angle (deg.)	Number of Diffuser Vanes	Number of Impeller Vanes
Point 1	7.5	10	9	6
Point 2	-2.5	5	9	4
Point 3	5	-7.5	9	5
Type_3 (original geometry)	0	0	9	5

A qualitative evaluation was also conducted for the original geometry Type_3 and the optimal geometry configuration 3 as shown in Fig. 20. For the original geometry, the pressure gradually increased in the impeller and reached a maximum value at the impeller outlet. It was observed that a kind of maximum pressure region was formed between the impeller and the diffuser, but the pressure in the diffuser region did not increase further and even decreased and moved towards the volute region. On the other hand, in the optimal geometry, the pressure increases in both the impeller and the diffuser regions passing into the volute region.

As far as velocities are concerned, it is observed that the original geometry contained low-speed regions, extending from the pressure side of one impeller blade towards the

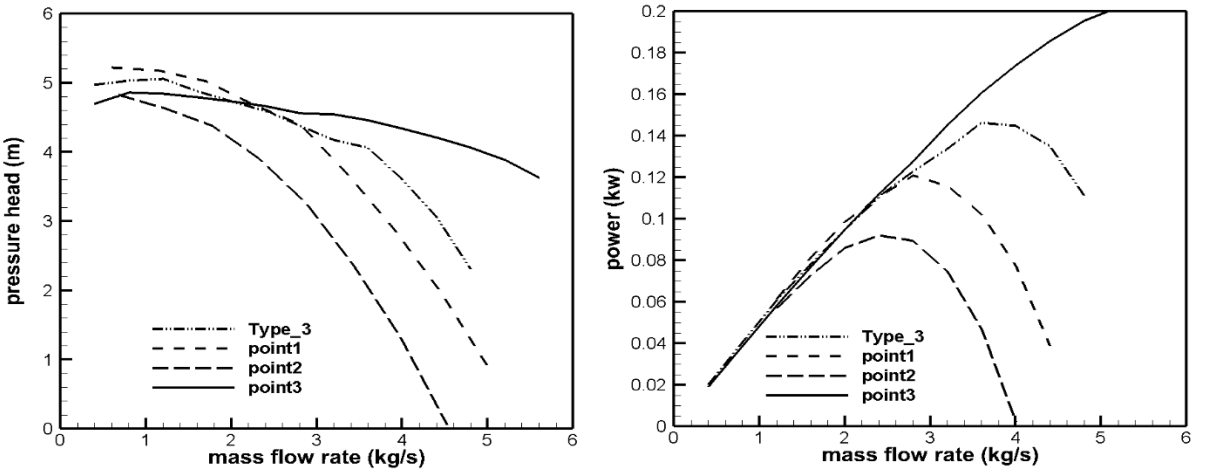

Fig. 19 Mass Flow Rate and Hydraulic Power Comparison of the cases Machine Learning (point 1, 2 and 3) to the original pump (Type_3).

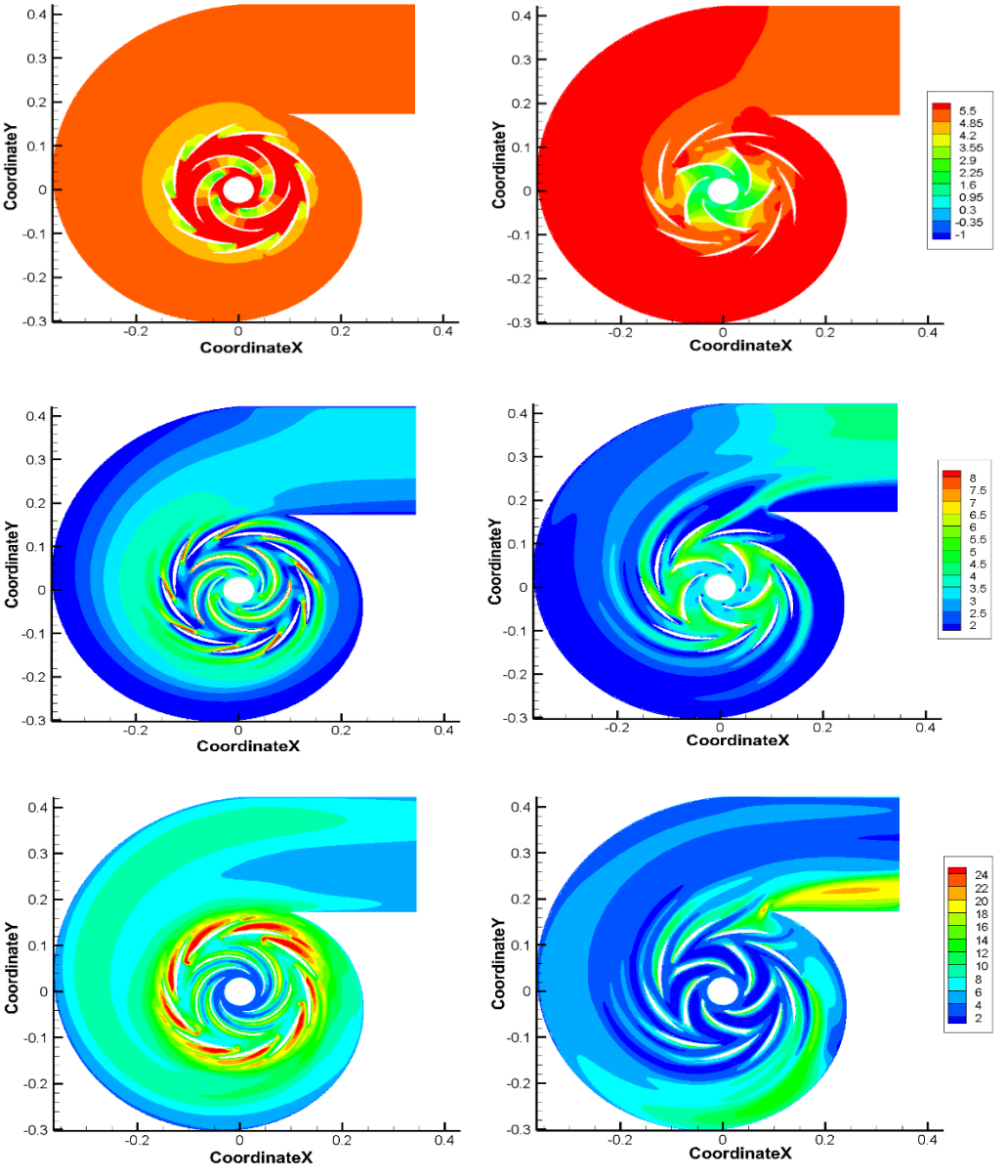

Fig. 20 Comparison of contours for original pump (left) vs optimal pump (right). (from top to bottom: pressure head (m), velocity magnitude (m/s) and turbulent intensity (%))

suction side of the other blade. However, for the optimal geometry, the low velocity regions have a much smaller area. Especially with the low wrap angle, the passage area becomes larger and the flow easily continues to the diffuser. Furthermore, despite having the same number of diffuser vanes, there are significant differences in the diffuser passages of the original and optimal geometries. Since the diffuser passages in the original geometry are narrower, formations containing the correct jet-wake mixture are formed which then move into the volute. In the diffuser passages of optimal geometry, the flow is observed to be more homogeneous.
Finally, turbulence intensity contours for two geometries are also reported in Fig. 20. In parallel with the jet-wake flow structure formed in the diffusers of the original geometry, significant turbulence occurred in these regions and reached levels of up to 30%. However, for the optimal geometry, it was observed that the turbulence was much lower in both the impeller and diffuser regions.

6. Conclusions

In this research, we have implemented a comprehensive approach to optimize centrifugal pump design and performance, leveraging numerical simulations, Exploratory Data Analysis (EDA), advanced machine learning models, and correlation analysis. Through extensive numerical simulations involving 693 distinct combinations of critical design parameters - the relative diffuser vane angle α_{dif}, number of diffuser vanes Z_d, number of impeller blades Z_i, and the impeller wrap angle α_{wrap} - we have obtained a rich dataset. This data provided insight into the complex interplay between these parameters and their impact on centrifugal pump performance, specifically pressure head and relative velocity angle. Subsequent EDA of the simulation data further illuminated the relationships and patterns within this data, leading to a more profound understanding of the pump's operational behaviour. This robust analytical approach enabled the extraction of meaningful insights from the data, thus paving the way for more accurate predictive modelling.
Our work has also demonstrated the efficacy of advanced machine learning models in predicting critical aspects of pump performance. The deep learning model developed for this study, trained on data generated from numerical simulations, successfully predicted pressure head and relative velocity angle. This achievement highlights the potential of machine learning in supplementing traditional design methodologies in turbomachinery, providing a pathway for more informed, data-driven decision-making in centrifugal pump design.

The correlation analysis presented in this study revealed significant relationships between pressure head and relative velocity angle, providing valuable insights for future centrifugal pump engineering efforts. By identifying and quantifying these correlations, we have introduced a new dimension to understanding the underlying physics of centrifugal pump operation.

In conclusion, the nexus of machine learning and numerical simulations, as demonstrated in this research, offers a potent tool for optimizing centrifugal pump performance as was reported in section 5.5 where the optimised configuration performed far superior than the baseline configuration. Future work can further refine the deep learning model with additional data and explore other machine learning techniques. The integration of these technological advancements in the centrifugal pump design process holds the promise of significant improvements in efficiency, reliability, and energy consumption, making a substantial contribution to the broader field of turbomachinery. For future analysis, it is recommended to focus on other design parameters such as, the impeller diameter, the inlet and outlet diameters of the diffuser vanes and the volute shape as new design parameters.

Conflict of Interest

There is no conflict of interest.

Supporting Information

Not applicable.

References

[1] A. Mohammed, Data driven-based model for predicting pump failures in the oil and gas industry, *Engineering Failure Analysis*, 2023, **145**, 107019, doi: 10.1016/j.engfailanal.2022.107019.
[2] P. F. Orrù, A. Zoccheddu, L. Sassu, C. Mattia, R. Cozza, S. Arena, Machine learning approach using MLP and SVM algorithms for the fault prediction of a centrifugal pump in the oil and gas industry, *Sustainability*, 2020, **12**, 4776, doi: 10.3390/su12114776.
[3] M. Neumann, T. Schäfer, A. Bieberle, U. Hampel, An experimental study on the gas entrainment in horizontally and vertically installed centrifugal pumps, *Journal of Fluids Engineering*, 2016, **138**, 091301, doi: 10.1115/1.4033029.
[4] T. Schäfer, A. Bieberle, M. Neumann, U. Hampel, Application of gamma-ray computed tomography for the analysis of gas holdup distributions in centrifugal pumps, *Flow Measurement and Instrumentation*, 2015, **46**, 262-267, doi: 10.1016/j.flowmeasinst.2015.06.001.
[5] W. Li, Model of flow in the side chambers of an industrial centrifugal pump for delivering viscous oil, *Journal of Fluids Engineering*, 2013, **135**, 051201, doi: 10.1115/1.4023664.
[6] W.-G. Li, Modeling viscous oil cavitating flow in a centrifugal pump, *Journal of Fluids Engineering*, 2016, **138**, 011303, doi: 10.1115/1.4031061.
[7] W. Wan, B. Zhang, X. Chen, Investigation on water hammer control of centrifugal pumps in water supply pipeline systems, *Energies*, 2018, **12**, 108, doi: 10.3390/en12010108.
[8] S. Pandey, R. P. Singh, P. S. Mahar, Optimal pipe sizing and operation of multistage centrifugal pumps for water

supply, *Journal of Pipeline Systems Engineering and Practice*, 2020, **11**, doi: 10.1061/(asce)ps.1949-1204.0000447.
[9] S. Bandi, J. Banka, A. Kumar, A. K. Rai, Effects of sediment properties on abrasive erosion of a centrifugal pump, *Chemical Engineering Science*, 2023, **277**, 118873, doi: 10.1016/j.ces.2023.118873.
[10] L. Deng, D. Zheng, J. Zhang, H. Yang, L. Wang, W. Wang, T. He, Y. Zhang, Treatment and utilization of swine wastewater - A review on technologies in full-scale application, *Science of The Total Environment*, 2023, **880**, 163223, doi: 10.1016/j.scitotenv.2023.163223.
[11] J. Pei, S. Yuan, J. Yuan, Fluid-structure coupling effects on periodically transient flow of a single-blade sewage centrifugal pump, *Journal of Mechanical Science and Technology*, 2013, **27**, 2015-2023, doi: 10.1007/s12206-013-0512-1.
[12] A. A. Noon, M.-H. Kim, Erosion wear on centrifugal pump casing due to slurry flow, *Wear*, 2016, **364-365**, 103-111, doi: 10.1016/j.wear.2016.07.005.
[13] G. Peng, X. Huang, L. Zhou, G. Zhou, H. Zhou, Solid-liquid two-phase flow and wear analysis in a large-scale centrifugal slurry pump, *Engineering Failure Analysis*, 2020, **114**, 104602, doi: 10.1016/j.engfailanal.2020.104602.
[14] F. Meng, H. Zhang, F. Yang, X. Hou, B. Lei, L. Zhang, Y. Wu, J. Wang, Z. Shi, Study of efficiency of a multistage centrifugal pump used in engine waste heat recovery application, *Applied Thermal Engineering*, 2017, **110**, 779-786, doi: 10.1016/j.applthermaleng.2016.08.226.
[15] B. Hu, H. Liu, R. Z. Wang, H. Li, Z. Zhang, S. Wang, A high-efficient centrifugal heat pump with industrial waste heat recovery for district heating, *Applied Thermal Engineering*, 2017, **125**, 359-365, doi: 10.1016/j.applthermaleng.2017.07.030.
[16] Y. Ganushchak, W. van Marken Lichtenbelt, T. van der Nagel, D. S. de Jong, Hydrodynamic performance and heat generation by centrifugal pumps, *Perfusion*, 2006, **21**, 373-379, doi: 10.1177/0267659106074003.
[17] F. Li, G. Zheng, Z. Tian, Optimal operation strategy of the hybrid heating system composed of centrifugal heat pumps and gas boilers, *Energy and Buildings*, 2013, **58**, 27-36, doi: 10.1016/j.enbuild.2012.09.044.
[18] Z. Shen, W. Chu, X. Li, W. Dong, Sediment erosion in the impeller of a double-suction centrifugal pump–A case study of the Jingtai Yellow River Irrigation Project, China, *Wear*, 2019, **422-423**, 269-279, doi: 10.1016/j.wear.2019.01.088.
[19] R. A. Carter, Prime Time for Pumps, *Engineering and Mining Journal*, 2016, **217**,30-32.
[20] K. D. Aaronson, M. S. Slaughter, L. W. Miller, E. C. McGee, W. G. Cotts, M. A. Acker, M. L. Jessup, I. D. Gregoric, P. Loyalka, O. H. Frazier, V. Jeevanandam, A. S. Anderson, R. L. Kormos, J. J. Teuteberg, W. C. Levy, D. C. Naftel, R. M. Bittman, F. D. Pagani, D. R. Hathaway, S. W. Boyce, Use of an intrapericardial, continuous-flow, centrifugal pump in patients awaiting heart transplantation, *Circulation*, 2012, **125**, 3191-3200, doi: 10.1161/circulationaha.111.058412.
[21] T. R. Karl, S. Sano, S. Horton, R. B. B. Mee, Centrifugal pump left heart assist in pediatric cardiac operations, *The Journal of Thoracic and Cardiovascular Surgery*, 1991, **102**, 624-630, doi: 10.1016/s0022-5223(20)31437-9.
[22] Gülich, J.F., Centrifugal pumps. Vol. 2. 2008: Springer.
[23] S. M. Hallaji, Y. Fang, B. K. Winfrey, Predictive maintenance of pumps in civil infrastructure: state-of-the-art, challenges and future directions, *Automation in Construction*, 2022, **134**, 104049, doi: 10.1016/j.autcon.2021.104049.
[24] P. Olszewski, Genetic optimization and experimental verification of complex parallel pumping station with centrifugal pumps, *Applied Energy*, 2016, **178**, 527-539, doi: 10.1016/j.apenergy.2016.06.084.
[25] S. Derakhshan, M. Pourmahdavi, E. Abdolahnejad, A. Reihani, A. Ojaghi, Numerical shape optimization of a centrifugal pump impeller using artificial bee colony algorithm, *Computers & Fluids*, 2013, **81**, 145-151, doi: 10.1016/j.compfluid.2013.04.018.
[26] A. Nourbakhsh, H. Safikhani, S. Derakhshan, The comparison of multi-objective particle swarm optimization and NSGA II algorithm: applications in centrifugal pumps, *Engineering Optimization*, 2011, **43**, 1095-1113, doi: 10.1080/0305215x.2010.542811.
[27] H. Safikhani, A. Khalkhali, M. Farajpoor, Pareto based multi-objective optimization of centrifugal pumps using CFD, neural networks and genetic algorithms, *Engineering Applications of Computational Fluid Mechanics*, 2011, **5**, 37-48, doi: 10.1080/19942060.2011.11015351.
[28] H.-S. Shim, K.-Y. Kim, Y.-S. Choi, Three-objective optimization of a centrifugal pump to reduce flow recirculation and cavitation, *Journal of Fluids Engineering*, 2018, **140**, 091202, doi: 10.1115/1.4039511.
[29] J. Pei, W. Wang, S. Yuan, Multi-point optimization on meridional shape of a centrifugal pump impeller for performance improvement, *Journal of Mechanical Science and Technology*, 2016, **30**, 4949-4960, doi: 10.1007/s12206-016-1015-7.
[30] Y. Zhang, S. Hu, J. Wu, Y. Zhang, L. Chen, Multi-objective optimization of double suction centrifugal pump using Kriging metamodels, *Advances in Engineering Software*, 2014, **74**, 16-26, doi: 10.1016/j.advengsoft.2014.04.001.
[31] Y. Xu, L. Tan, S. Cao, W. Qu, Multiparameter and multiobjective optimization design of centrifugal pump based on orthogonal method, *Proceedings of the Institution of Mechanical Engineers, Part C: Journal of Mechanical Engineering Science*, 2017, **231**, 2569-2579, doi: 10.1177/0954406216640303.
[32] L. Zhou, W. Shi, S. Wu, Performance optimization in a centrifugal pump impeller by orthogonal experiment and numerical simulation, *Advances in Mechanical Engineering*, 2013, **5**, 385809, doi: 10.1155/2013/385809.
[33] J. Pei, T. Yin, S. Yuan, W. Wang, J. Wang, Cavitation optimization for a centrifugal pump impeller by using orthogonal design of experiment, *Chinese Journal of Mechanical Engineering*, 2017, **30**, 103-109, doi:

10.3901/cjme.2016.1024.125.
[34] J. Pei, W. Wang, M. K. Osman, X. Gan, Multiparameter optimization for the nonlinear performance improvement of centrifugal pumps using a multilayer neural network, *Journal of Mechanical Science and Technology*, 2019, **33**, 2681-2691, doi: 10.1007/s12206-019-0516-6.
[35] J. Wu, Elimination of adverse leakage flow in a miniature pediatric centrifugal blood pump by computational fluid dynamics-based design optimization, *ASAIO journal*, 2005, **51**, 636-643, doi: 10.1097/01.mat.0000178966.79876.3d.
[36] N. S. Ranawat, J. Prakash, A. Miglani, P. K. Kankar, Performance evaluation of LSTM and Bi-LSTM using non-convolutional features for blockage detection in centrifugal pump, *Engineering Applications of Artificial Intelligence*, 2023, **122**, 106092, doi: 10.1016/j.engappai.2023.106092.
[37] X. Ping, F. Yang, H. Zhang, J. Zhang, W. Zhang, G. Song, Introducing machine learning and hybrid algorithm for prediction and optimization of multistage centrifugal pump in an ORC system, *Energy*, 2021, **222**, 120007, doi: 10.1016/j.energy.2021.120007.
[38] A. Kumar, C. P. Gandhi, Y. Zhou, R. Kumar, J. Xiang, Improved deep convolution neural network (CNN) for the identification of defects in the centrifugal pump using acoustic images, *Applied Acoustics*, 2020, **167**, 107399, doi: 10.1016/j.apacoust.2020.107399.
[39] J. Zhao, J. Pei, J. Yuan, W. Wang, Energy-saving oriented optimization design of the impeller and volute of a multi-stage double-suction centrifugal pump using artificial neural network, *Engineering Applications of Computational Fluid Mechanics*, 2022, **16**, 1974-2001, doi: 10.1080/19942060.2022.2127913.
[40] Y. Hou, Y. Wang, Y. Pan, W. He, W. Huang, P. Wu, D. Wu, Vibration-based incipient surge detection and diagnosis of the centrifugal compressor using adaptive feature fusion and sparse ensemble learning approach, *Advanced Engineering Informatics*, 2023, **56**, 101947, doi: 10.1016/j.aei.2023.101947.
[41] S. Tang, Y. Zhu, S. Yuan, An adaptive deep learning model towards fault diagnosis of hydraulic piston pump using pressure signal, *Engineering Failure Analysis*, 2022, **138**, 106300, doi: 10.1016/j.engfailanal.2022.106300.
[42] W. Zhang, L. An, X. Li, F. Chen, L. Sun, X. Wang, J. Cai, Adjustment method and energy consumption of centrifugal pump based on intelligent optimization algorithm, *Energy Reports*, 2022, **8**, 12272-12281, doi: 10.1016/j.egyr.2022.09.031.
[43] N. Dutta, S. Umashankar, V. K. A. Shankar, S. Padmanaban, Z. Leonowicz, P. Wheeler, Centrifugal pump cavitation detection using machine learning algorithm technique, 2018 IEEE International Conference on Environment and Electrical Engineering and 2018 IEEE Industrial and Commercial Power Systems Europe (EEEIC / I&CPS Europe). Palermo, Italy. IEEE, 2018.
[44] R. Tiwari, D. J. Bordoloi, A. Dewangan, Blockage and cavitation detection in centrifugal pumps from dynamic pressure signal using deep learning algorithm, *Measurement*, 2021, **173**, 108676, doi: 10.1016/j.measurement.2020.108676.
[45] A. K. Panda, J. S. Rapur, R. Tiwari, Prediction of flow blockages and impending cavitation in centrifugal pumps using Support Vector Machine (SVM) algorithms based on vibration measurements, *Measurement*, 2018, **130**, 44-56, doi: 10.1016/j.measurement.2018.07.092.
[46] M. J. Hasan, A. Rai, Z. Ahmad, J.-M. Kim, A fault diagnosis framework for centrifugal pumps by scalogram-based imaging and deep learning, *IEEE Access*, 2021, **9**, 58052-58066, doi: 10.1109/ACCESS.2021.3072854.
[47] O. Surucu, S. A. Gadsden, J. Yawney, Condition Monitoring using Machine Learning: a Review of Theory, Applications, and Recent Advances, *Expert Systems with Applications*, 2023, **221**, 119738, doi: 10.1016/j.eswa.2023.119738.
[48] M. Sinha, A. Pinarbasi, J. Katz, The flow structure during onset and developed states of rotating stall within a vaned diffuser of a centrifugal pump, *Journal of Fluids Engineering*, 2001, **123**, 490-499, doi: 10.1115/1.1374213.
[49] Fluent, A., Gambit User's Guide. Fluent Inc, 2005.
[50] A. Fluent, 6.3, 2006, FLUENT 6.3 User's Guide, Fluent. Inc., Lebanon, NH, 2014.
[51] A. J. Chorin, Numerical solution of the Navier-Stokes equations, *Mathematics of Computation*, 1968, **22**, 745-762, doi: 10.1090/s0025-5718-1968-0242392-2.
[52] R. I. Issa, Solution of the implicitly discretised fluid flow equations by operator-splitting, *Journal of Computational Physics*, 1986, **62**, 40-65, doi: 10.1016/0021-9991(86)90099-9.
[53] S. Patankar, Numerical Heat Transfer and Fluid Flow: CRC Press, 1980.
[54] F. Menter, R. Langtry, S. Likki, Y. Suzen, P. Huang, S. Völker, A correlation-based transition model using local variables: part I—model formulation, 2004.
[55] K. M. Guleren, I. Afgan, A. Turan, Predictions of turbulent flow for the impeller of a NASA low-speed centrifugal compressor, *Journal of Turbomachinery*, 2010, **132**, 1, doi: 10.1115/1.3140824.
[56] A. Filippone, I. Afgan, Orthogonal blade-vortex interaction on a helicopter tail rotor, *AIAA Journal*, 2008, **46**, 1476-1489, doi: 10.2514/1.32690.
[57] I. Afgan, J. McNaughton, S. Rolfo, D. D. Apsley, T. Stallard, P. Stansby, Turbulent flow and loading on a tidal stream turbine by LES and RANS, *International Journal of Heat and Fluid Flow*, 2013, **43**, 96-108, doi: 10.1016/j.ijheatfluidflow.2013.03.010.